Hindawi
Shock and Vibration
Volume 2023, Article ID 6644285, 17 pages
https://doi.org/10.1155/2023/6644285

Research Article

Stability Analysis of Roof and Rib and Source Control Countermeasures of Ultrahigh Roadway in Deep Coal Mine

Ye Zhu,[1,2] **Xinzhu Hua**,[2] **and Weiyu Li**[1]

[1]*State Key Laboratory of Mining Response and Disaster Prevention and Control in Deep Coal Mines, Anhui University of Science and Technology, Huainan 232001, China*
[2]*School of Mining Engineering, Anhui University of Science and Technology, Huainan 232001, China*

Correspondence should be addressed to Ye Zhu; zhuye0421@163.com

Received 23 November 2022; Revised 28 February 2023; Accepted 6 March 2023; Published 4 April 2023

Academic Editor: Antonio Giuffrida

Driven by the high original rock stress and engineering disturbance, the ultrahigh roadways of about 7~8 m appear in the deep coal mine. Based on the field measured data, the stability in different zones of roof and rib is divided. From shallow to deep, the roof forms potential leakage and falling zone, metastable zone, and stable zone, and the coal rib forms potential spalling zone, crack developed zone, and transition zone. Based on the theory of transverse isotropy, the mechanical analysis model of layered roof is established, the real stress state at any point of layered roof is deduced, the roof failure criterion is constructed, and the theoretical solution of the failure depth of layered roof is obtained. The mechanical model of pillar bar of the splitting coal body in the potential spalling zone is established, and the deflection deformation expression of the pillar bar is derived. In view of the deformation and failure characteristics of the roof and rib, this paper puts forward the cooperative integrated support technology based on high-strength prestressed cables and deep-shallow hole grouting, which effectively reduce the hidden danger of roof falling and eliminate the formation of ultrahigh roadway from the source.

1. Introduction

The in situ stress level increases with the increase of the buried depth of the roadway, and the surrounding rock shows the property of soft rock. Under the influence of the engineering excavation disturbance, the environment of the roadway tends to be complicated, and the risk potential of the roof falling and the rib spalling is increased [1]. On the one hand, roof falling and rib spalling seriously threaten the safe production of the mine; on the other hand, they block the roadway, restrict the operation of the production system, and seriously threaten the efficient production of the mine [2–4]. At the same time, the frequent roof falling forms ultrahigh roadway, and the support cost is huge, which seriously affects the benefit of the mine.

Roof and rib are the weak links of surrounding rock bearing structure of deep roadway and are the key factors that restrict the long-term stability of deep roadway. At present, relevant scholars have carried out a lot of research work on the stability and control technology of the roof-rib bearing system and have achieved fruitful research results. An et al. took the thick-coal-roof roadways as the research object, studied the evolution law of the roof failure area under the condition of insufficient support, and proposed an improved support with thick anchoring structure and roof reinforcement, which effectively reduced the damage height of the thick coal roof [5]. Bai et al. studied the process of progressive roof failure in a wide coal roadway from water-rich roofs based on the UDEC method. The numerical results revealed that the progressive failure mechanism was characterized by an initial fracturing of the roof due to strength degradation, which was followed by significant dilation as fractures grew. The large span of the roadway further contributed to the roof failure process [6]. On the basis of fully considering the actual characteristics of coal seam and roof, Yu et al. established a mechanical calculation model of compound roof roadway by using elastic mechanics theory, deduced the bed separation and instability

limit load expressions of compound roof, and proposed the targeted stability control technology for roadways with a compound roof, which effectively improved the overall stability of the roadway [7]. Jiang et al. simplified the immediate roof stratum as an elastic beam supported on a Winkler-type foundation, then obtained the bending stress and deflection of the roof beam, and considered that the elastic coefficient of the coal seam is the key factor for the deformation and potential damage of the roof [8]. Liu et al. regarded the immediate roof as an elastic body, established the mechanical model of the immediate roof in the whole process of gob-side entry retaining by roof cutting, analyzed the stress characteristics of the immediate roof, and finally obtained the relationship between the deformation of the immediate roof and the stiffness of the support system [9]. Based on the infinite plate theory, Yu et al. obtained the expressions of deflection and bed separation of the composite roof and determined the critical load expression of each delamination, and the influence of roadway width, overlying strata load, elastic modulus, shape parameters, and scale parameters on the stability of composite roof was explored [10]. Gao et al. used a novel UDEC Trigon approach to conduct numerical simulation and truly reproduced the squeezing failure process of roof rock under high stress environment [11]. Wang et al. undertook an investigation to study driving force of roof fall in a geologically complex zone, and the results revealed that the driving force of the roof fall was that the high levels of horizontal tectonic stress and fault slip were induced by mining activities [12].

Based on the physical and mechanical parameters, in situ stress measurements, and the failure characteristics of the roadway, Sun et al. proposed the yielding bolt-grouting support design to restrict the deformation of roadway ribs [13]. Wu et al. used field tests and numerical modeling to study the initiation, propagation, and failure of cracks within the gob-side coal pillar rib, and the failure mechanism of coal pillar rib is revealed [14]. Based on Hoek–Brown and Mohr–Coulomb strength criteria, De-Feng et al. deduced the equation of normal stress and limit equilibrium zone width of slip surface of roadway rib related to engineering disturbance degree and geological strength index of rock mass and analyzed the integrity of roadway rib [15]. De-Chao et al. established a mechanical analysis model considering the softening characteristics of the coal rib and obtained the stress, deformation, and failure characteristics of the gob side entry retaining coal rib [16]. Ren-Liang et al. put forward the strong support theory for sidewall in coal roadway on the basis of analyzing the mechanism of coal rib damage and reinforcement and obtained good application effect in engineering practice [17, 18].

The existing studies have analyzed the stability of roof and rib from different angles and methods and put forward targeted control countermeasures for specific engineering cases. However, as a special kind of engineering research object, the formation mechanism of ultrahigh roadway is rarely involved in the existing research, so it is difficult to fundamentally inhibit the formation of ultrahigh roadway. Therefore, it is of great engineering significance to explore the formation mechanism of ultrahigh roadway by theoretical analysis and numerical calculation based on the field investigation data and engineering geological data, so as to put forward targeted control measures.

2. Project Background

2.1. Engineering Geological Conditions. The Zhaozhuang Mine in Changzhi, Shanxi, China, currently mainly mines 3# coal seam, which is nearly horizontal, with an average thickness of 4.6 m and an average burial depth of more than 600 m. The development roadways and the mining roadways are arranged in the coal seam and are driven along the roof of the coal seam. The uniaxial compressive strength of the coal is only 2.1~13.2 MPa, so the coal rib is soft and broken, with developed cracks and poor stability. The immediate roof is mudstone or sandy mudstone and locally siltstone, which has developed bedding, forming a longitudinal discontinuous structure, resulting in poor roof integrity. The main roof is fine sandstone with thick-layered structure and high rock strength. The immediate floor is mudstone or carbonaceous mudstone, with thin coal interlayer locally. The columnar information of the roof and floor rocks is shown in Figure 1(a). The immediate roof and floor are mudstone and sandy mudstone with weak mechanical properties. The rock mass has obvious layered characteristics and low bearing capacity. With the development and penetration of surrounding rock cracks, the roof will sink violently and even lead to roof collapse. The integrity of coal rib is also poor. Under the influence of overburden pressure, the coal rib is seriously squeezed, the phenomenon of rib spalling occurs frequently, a large number of supporting members fail, and the stability of the coal rib is significantly reduced.

As shown in Figure 1(b), the content of clay minerals in mudstone and sandy mudstone is as high as 56.4% and 46.3%, and the content of illite montmorillonite mixed layer in clay minerals is 41% and 34.4%, respectively. Water molecules can easily enter the crystal lattice of montmorillonite, resulting in changes in the thickness of its crystal structure, which is macroscopically manifested as rock expansion. Montmorillonite has very strong ion exchange performance and good hydrophilicity. It is very easy to show argillization and disintegration after encountering with water, resulting in great attenuation of rock strength. The reduction of bearing capacity and the occurrence of layer separation induce the instability of roof rock mass.

2.2. Deformation and Failure Characteristics of Surrounding Rock. After the roadway is excavated, the borehole imager is used to detect the internal structure of the surrounding rock. The roof rock structure is shown in Figure 2(a). The shallow roof crack within 0~4 m is highly developed, and the layer separation phenomenon is obvious, forming a potential leakage and falling zone. The integrity of the roof rock within the range of 4~8 m is gradually improved, forming a metastable zone. Due to the existence of weak interlayer, there are significant open cracks in local areas. The roof rock beyond 8 m is stable, forming a stable zone, which is the main bearing structure of the roof. The internal structure of the

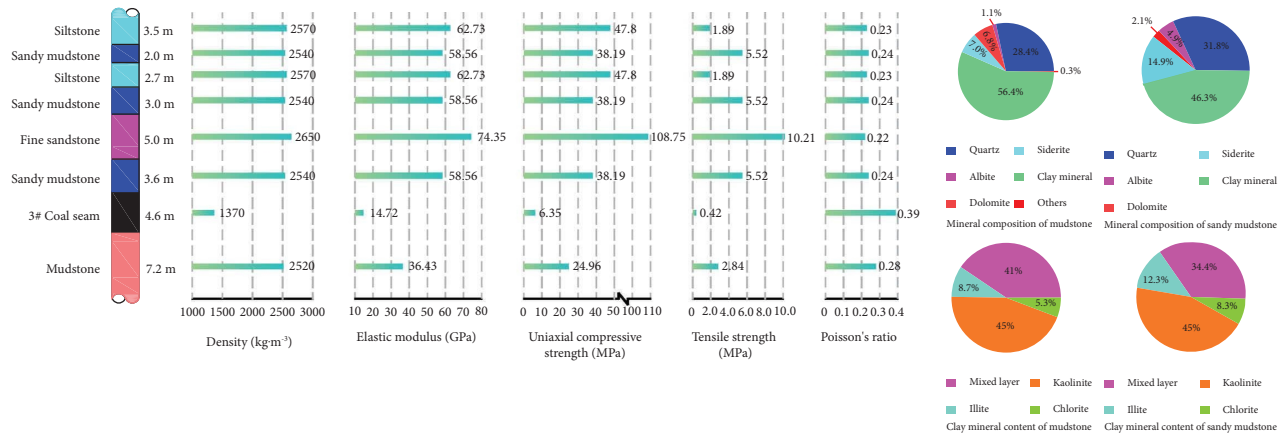

(a) (b)

Figure 1: Rock properties of roof and floor: (a) rock stratum histogram; (b) mineral composition.

coal rib is shown in Figure 2(b). Due to the low bearing capacity of the coal body, after the roadway is excavated, potential spalling zone, crack developed zone, and transition zone are formed from shallow to deep in the coal rib. The destruction of the shallow coal rib increases the real span of the roadway and further reduces the stability of the roof.

2.3. Formation Mechanism of Ultrahigh Roadway. As shown in Figure 3(a), the roof structure and the working conditions of supporting members exposed after the roadway roof falling. The roof has a remarkable layered structure, with a layer thickness of about 0.2 m and poor interlayer bonding performance. Under the pressure of the overlying strata, separation and dislocation occur in the vertical direction and horizontal direction of the layered roof, respectively, resulting in tensile fracture, shear fracture, and tensile shear composite fracture of the cables. The interface element in FLAC3D is used to construct the interlayer structural plane and simulate the layered characteristics of the roof rock mass. According to previous studies, the elastic modulus, cohesion, and tensile strength are taken as 0.2 times the experimental value, and the Poisson's ratio is taken as 1.2 times the experimental value. The calculated failure mode of the layered roof is shown in Figure 3(b). The roof presents significant progressive failure layer by layer. The discontinuity of layered rock mass results in the discontinuity of its deformation. There is a large-scale separation zone in the roof, forming a potential caving arch structure. With the gradual development of the rock mass bed separation within the potential caving arch, the rock mass in the arch shows structural instability, forming an ultrahigh roadway with a height of about 7~8 m (Figure 3(c)).

3. Roof Stability Analysis

3.1. Stress Distribution Characteristics. The coal bearing rock series formed a typical layered structure during the deposition process [19]. The mechanical behavior of layered rock mass is affected by the weak structural plane and has significant anisotropy. The transverse isotropic body can well characterize the mechanical behavior of layered rock mass. In the transverse isotropic plane, the layered rock mass has the same mechanical properties, while in the direction perpendicular to the plane, the rock mass shows another property. The elastic constitutive relationship of a transversely isotropic body is expressed as [20, 21].

$$\begin{bmatrix} \varepsilon_{xx} \\ \varepsilon_{zz} \\ \gamma_{xz} \end{bmatrix} = \begin{bmatrix} a_{11} & a_{12} & 0 \\ a_{12} & a_{22} & 0 \\ 0 & 0 & a_{66} \end{bmatrix} \begin{bmatrix} \sigma_{xx} \\ \sigma_{zz} \\ \tau_{xz} \end{bmatrix}, \tag{1}$$

where $a_{11} = (1-\mu)/E_H$, $a_{12} = -\mu_V(1+\mu_H)/E_V$, $a_{22} = (1-\mu/E_H)/E_V$, and $a_{66} = 1/G_V$. Here, E_H and E_V are horizontal and vertical elastic modulus, μ_H is Poisson's ratio of vertical strain caused by horizontal strain, μ_V is Poisson's ratio of horizontal strain caused by vertical strain, and G_V is the shear modulus perpendicular to the xy plane.

Ignoring the volume force, it is assumed that the material of a half plane body conforms to the transverse isotropic constitutive relation. Under the action of concentrated force on the boundary, the compatible equation expressed by the stress function in the plane problem can be expressed as

$$a_{11}\frac{\partial^4\Phi}{\partial y^4} + (2a_{12} + a_{66})\frac{\partial^4\Phi}{\partial x^2\partial y^2} + a_{22}\frac{\partial^4\Phi}{\partial x^4} = 0. \tag{2}$$

By solving equation (2), the stress component at any point after the transversely isotropic half-plane body is subjected to the concentrated force perpendicular to the isotropic plane can be obtained as follows:

$$\begin{cases} \sigma_x = \dfrac{F}{\pi}\left[\dfrac{K_{\mathrm{I}}c^3 z}{x^2+(cz)^2} - \dfrac{K_{\mathrm{II}}f^3 z}{x^2+(fz)^2}\right], \\ \sigma_z = -\dfrac{F}{\pi}\left[\dfrac{K_{\mathrm{I}}cz}{x^2+(cz)^2} - \dfrac{K_{\mathrm{II}}fz}{x^2+(fz)^2}\right], \\ \tau_{xz} = -\dfrac{F}{\pi}\left[\dfrac{K_{\mathrm{I}}cx}{x^2+(cz)^2} - \dfrac{K_{\mathrm{II}}fx}{x^2+(fz)^2}\right], \end{cases} \tag{3}$$

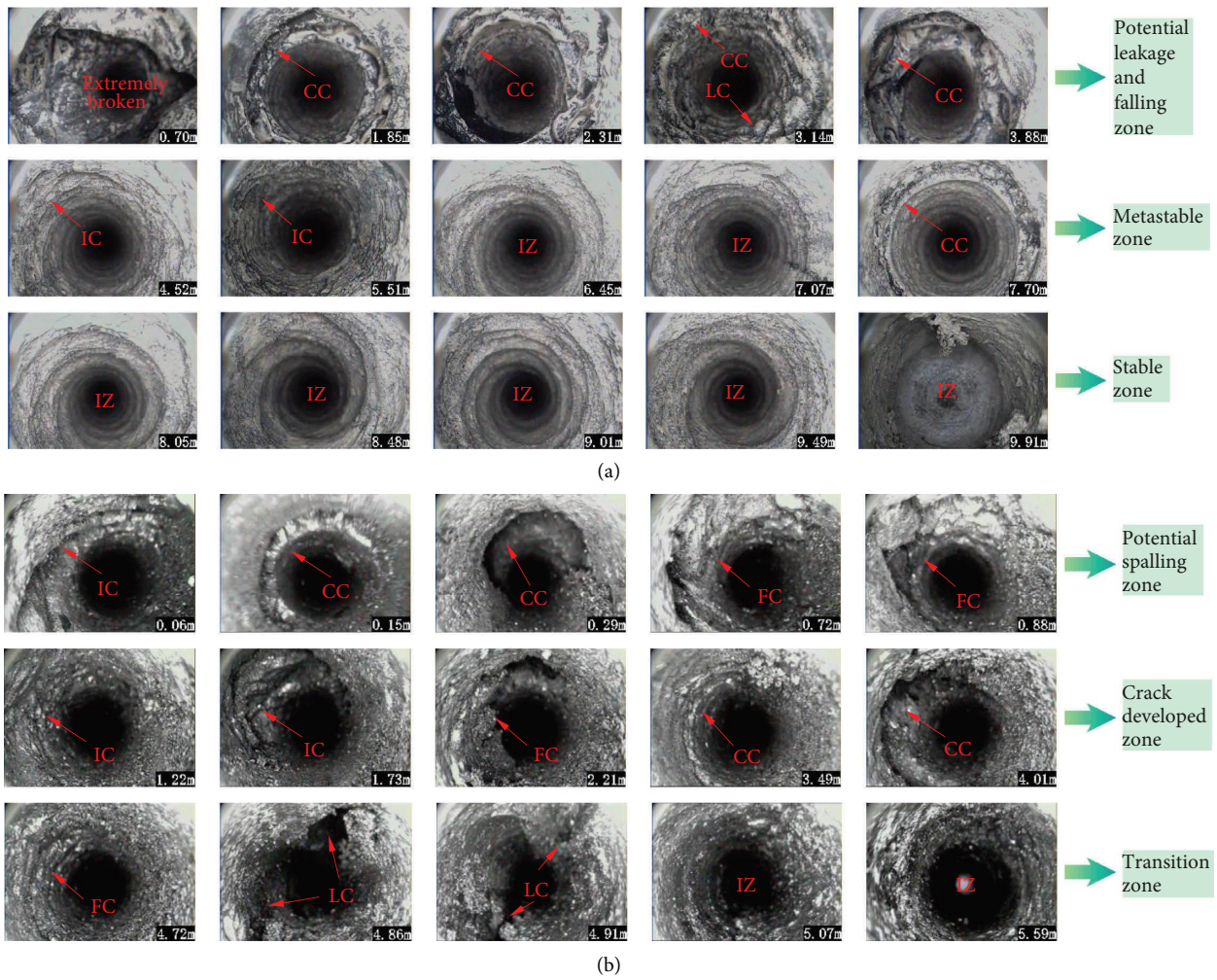

Figure 2: Internal structure of surrounding rock: (a) internal structure of roof; (b) internal structure of coal rib (CC means circumferential crack; LC means longitudinal crack; IC means interlaced crack; IZ means intact zone; FC means fracture zone).

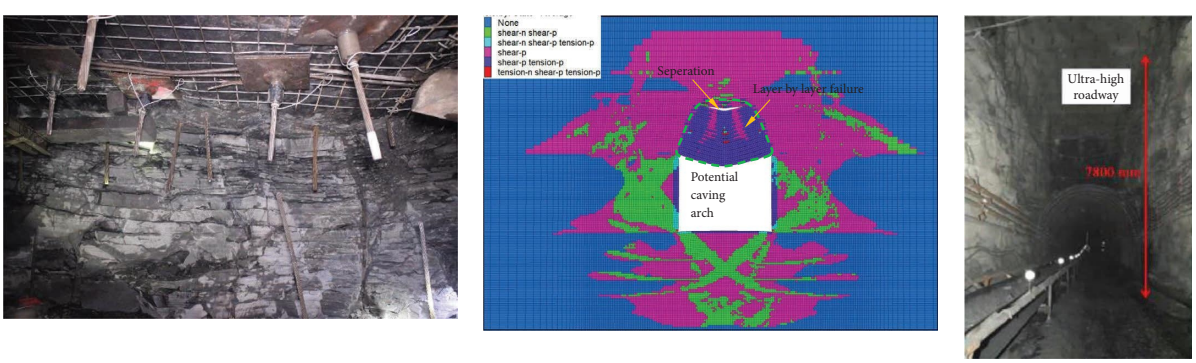

Figure 3: Formation mechanism of ultrahigh roadway: (a) exposed roof; (b) roof failure mode; (c) ultrahigh roadway.

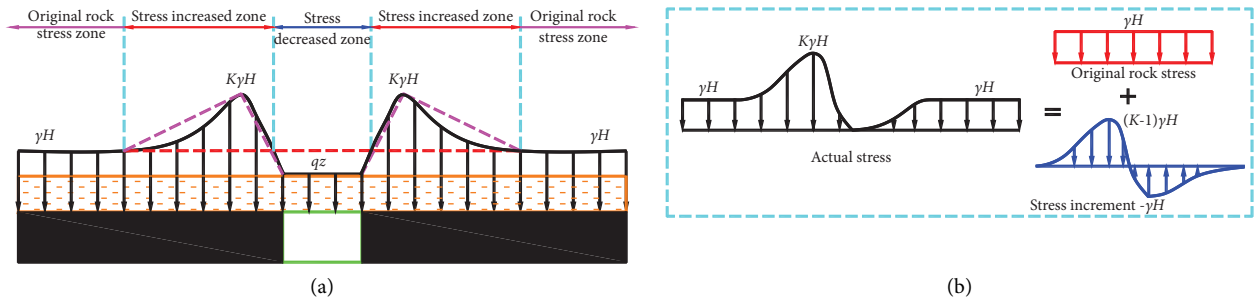

Figure 4: Stress distribution of surrounding rock: (a) stress curve; (b) stress composition.

where $K_{\mathrm{I}} = f/(c-f)$, $K_{\mathrm{II}} = c/(c-f)$, and the expressions of c and f are

$$\left.\begin{matrix} c \\ f \end{matrix}\right\} = \sqrt{\frac{a_{66}/2 + a_{12} \pm \sqrt{(a_{66}/2 + a_{12})^2 - a_{11}a_{22}}}{a_{11}}}. \tag{4}$$

According to formula (3), the stress component at any point of a transversely isotropic half-plane body under linear load can be obtained by superposition principle.

Excavating the roadway in the undisturbed natural rock mass breaks the stress balance state of the original rock, and the original rock stress is redistributed. The surrounding rock of the roadway forms stress-decreased zone, stress-increased zone, and original rock stress zone in turn. The stress distribution of surrounding rock is shown in Figure 4(a). The original rock stress is γH. The peak stress of surrounding rock on both sides of the roadway is $K_{\gamma H}$, where K represents the stress concentration factor. As shown in Figure 4(b), according to the principle of stress superimposition, the actual stress at any point of the roof can be characterized as the sum of the original rock stress and the additional stress caused by the stress increment. The original rock stress of the roadway can be calculated according to the measured data or the buried depth of the roadway according to formula (5). Therefore, under the action of overburden pressure, the stress solution of layered roof can be reduced to the solution of additional stress:

$$\begin{cases} \sigma_v = \gamma H, \\ \sigma_H = \lambda \gamma H. \end{cases} \tag{5}$$

The mechanical model of stress increment as shown in Figure 5 is established by taking the right direction parallel to the roof as the positive direction of the x-axis and the right direction perpendicular to the roof as the positive direction of the z-axis, where L_1 and L_4 represent the distance between the original rock stress boundary and the roof stress peak point, L_2 and L_3 represent the distance between the roof stress peak point and the coal rib, and B represents the width of the roadway. The expression of load in each interval can be expressed as

$$q_i = A_i x + B_i, \ (i = 1 \sim 5), \tag{6}$$

where $A_1 = (K-1)\gamma H/L_1$, $B_1 = A_1(L_1 + L_2)$, $A_2 = (q_z - K_{\gamma H})/L_2$, $B_2 = q_z - \gamma H$, $A_3 = 0$, $B_3 = q_z - \gamma H$, $A_4 = (K_{\gamma H} - q_z)/L_3$, $B_4 = q_z - \gamma H - BA_4$, $A_5 = -(K-1)\gamma H/L_4$, and $B_5 = -A_5(B + L_3 + L_4)$.

We take the microsegment $\mathrm{d}\xi$ at the distance $|\xi|$ from the coordinate origin, and the load within the microsegment can be simplified as the concentrated force, that is, $\mathrm{d}F = q\mathrm{d}\xi$. The stress generated by $\mathrm{d}F$ at any point $M(x, z)$ of the lower rock layer can be solved according to formula (3). Here, the vertical and horizontal distances between the action point of $\mathrm{d}F$ and the point M are, respectively, expressed as $|z|$ and $|x - \xi|$. Therefore, the additional stress generated by $\mathrm{d}F$ at point M is

$$\begin{cases} d\sigma_x = \dfrac{(A_1\xi + B_1)\mathrm{d}\xi}{\pi}\left[\dfrac{K_{\mathrm{I}}c^3 z}{(x-\xi)^2 + (cz)^2} - \dfrac{K_{\mathrm{II}}f^3 z}{(x-\xi)^2 + (fz)^2}\right], \\ d\sigma_z = -\dfrac{(A_1\xi + B_1)\mathrm{d}\xi}{\pi}\left[\dfrac{K_{\mathrm{I}}cz}{(x-\xi)^2 + (cz)^2} - \dfrac{K_{\mathrm{II}}fz}{(x-\xi)^2 + (fz)^2}\right], \\ d\tau_{xz} = -\dfrac{(A_1\xi + B_1)\mathrm{d}\xi}{\pi}\left[\dfrac{K_{\mathrm{I}}c(x-\xi)}{(x-\xi)^2 + (cz)^2} - \dfrac{K_{\mathrm{II}}f(x-\xi)}{(x-\xi)^2 + (fz)^2}\right]. \end{cases} \tag{7}$$

The stress caused by all the small concentrated forces in the interval at point M is superimposed, that is, formula (7) is integrated in the load action interval, and the additional stress value of point M under the linear load in the integration interval can be obtained. Each integral interval has the same solution process except that the upper and lower

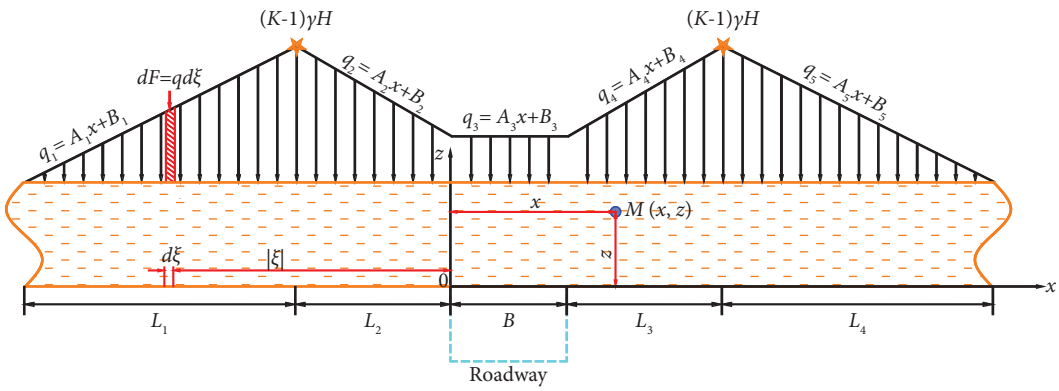

Figure 5: Stress increment mechanical model.

limits of integration are different. The $[-L_1\text{-}L_2, -L_2]$ interval is taken as an example for explanation.

$$\begin{cases} \Delta\sigma_{x1} = \dfrac{(A_1x+B_1)K_1c^2}{\pi}\left(\arctan\dfrac{x+L_1+L_2}{cz} - \arctan\dfrac{x+L_2}{cz}\right) + \dfrac{A_1K_1c^3z}{2\pi}\left\{\ln\left[(x+L_2)^2+(cz)^2\right] - \ln\left[(x+L_1+L_2)^2+(cz)^2\right]\right\} \\ -\dfrac{(A_1x+B_1)K_{II}f^2}{\pi}\left(\arctan\dfrac{x+L_1+L_2}{fz} - \arctan\dfrac{x+L_2}{fz}\right) - \dfrac{A_1K_{II}f^3z}{2\pi}\left\{\ln\left[(x+L_2)^2+(fz)^2\right] - \ln\left[(x+L_1+L_2)^2+(fz)^2\right]\right\} \\ \Delta\sigma_{z1} = -\dfrac{K_1(A_1x+B_1)}{\pi}\left(\arctan\dfrac{x+L_1+L_2}{cz} - \arctan\dfrac{x+L_2}{cz}\right) - \dfrac{A_1K_1cz}{2\pi}\left\{\ln\left[(x+L_2)^2+(cz)^2\right] - \ln\left[(x+L_1+L_2)^2+(cz)^2\right]\right\} \\ +\dfrac{K_{II}(A_1x+B_1)}{\pi}\left(\arctan\dfrac{x+L_1+L_2}{fz} - \arctan\dfrac{x+L_2}{fz}\right) + \dfrac{A_1K_{II}fz}{2\pi}\left\{\ln\left[(x+L_2)^2+(fz)^2\right] - \ln\left[(x+L_1+L_2)^2+(fz)^2\right]\right\} \\ \Delta\tau_{xz1} = -\dfrac{K_1c(A_1x+B_1)}{2\pi}\left\{\ln\left[(x+L_1+L_2)^2+(cz)^2\right] - \ln\left[(x+L_2)^2+(cz)^2\right]\right\} + \dfrac{K_1cA_1}{\pi}L_1 - \dfrac{K_1c^2A_1z}{\pi}\left(\arctan\dfrac{x+L_1+L_2}{cz} - \arctan\dfrac{x+L_2}{cz}\right) \\ +\dfrac{K_{II}f(A_1x+B_1)}{2\pi}\left\{\ln\left[(x+L_1+L_2)^2+(fz)^2\right] - \ln\left[(x+L_2)^2+(fz)^2\right]\right\} - \dfrac{K_{II}fA_1}{\pi}L_1 + \dfrac{K_{II}f^2A_1z}{\pi}\left(\arctan\dfrac{x+L_1+L_2}{fz} - \arctan\dfrac{x+L_2}{fz}\right). \end{cases} \tag{8}$$

The additional stress value of the roof under the stress increment can be obtained by superimposing the integration results of each interval. The sum of the additional stress and the original rock stress is the actual stress state of the roof, namely,

$$\begin{cases} \sigma_x = \sum_{i=1}^{5}\Delta\sigma_{xi} + \lambda\gamma H, \\ \sigma_z = \sum_{i=1}^{5}\Delta\sigma_{zi} + \gamma H, \\ \tau_{xz} = \sum_{i=1}^{5}\Delta\tau_{xzi}. \end{cases} \tag{9}$$

According to the engineering geological data, the calculation parameters are selected as follows: roadway span $B = 5.5$ m; the roof load is distributed symmetrically, $L_1 = L_4 = 10$ m, $L_2 = L_3 = 5$ m; average volumetric weight of rock $\gamma = 25$ kN/m^3; roadway buried depth $H = 670$ m; stress concentration coefficient $K = 2.0$; lateral stress coefficient $\lambda = 1.2$. According to formula (9), the stress distribution of the roof under the influence of roadway excavation is calculated by MATLAB.

The stress cloud of the roof after the roadway is excavated is shown in Figure 6, which is distributed symmetrically. As shown in Figures 6(a) and 6(b), the vertical stress and horizontal stress, respectively, form stress concentration zones in the roof above the solid coal and unloading zones in the roof above the roadway. The influence range of stress concentration zone and unloading zone of vertical stress is significantly larger than that of horizontal stress. With the increase of depth, the vertical stress and horizontal stress gradually return to the original rock stress level. Taking the roadway center line as the boundary, as shown in Figure 6(c), the shear stress forms four symmetrically distributed shear stress concentration zones in the roof above the solid coal on both sides. The shear stress concentration zone near the roadway is defined as zone I, and the zone far away is defined as zone II. The existence of zone I is the direct cause of roadway upper corners failure, and its stress concentration is significantly greater than that of zone II.

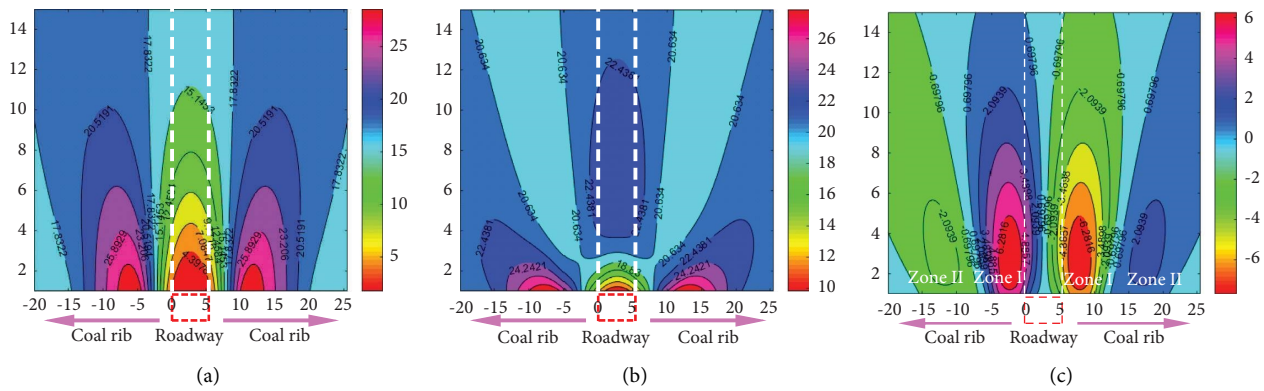

Figure 6: Stress cloud of roof: (a) vertical stress; (b) horizontal stress; (c) shear stress.

We extract the stress curves of different layers roof from the stress cloud, as shown in Figure 7. Here, we define the roof unloading coefficient K' = (original rock stress – actual stress)/original rock stress. As shown in Figure 7(a), at 0.5 m above the roadway roof, the vertical stress unloading coefficient is 0.91, which indicates that the roof rock mass is seriously damaged and the bearing capacity is basically lost. As the depth increases from 0.5 m to 3.5 m, the unloading coefficient of the rock mass above the roadway gradually decreases from 0.91 to 0.68, and the vertical stress gradually recovers, indicating that the bearing capacity of the rock mass gradually increases. At the same time, the vertical stress concentration coefficient of the roof above the coal body decreases from 1.93 to 1.59, and the stress concentration degree gradually decreases.

As shown in Figure 7(b), with the increase of the depth, the unloading coefficient of the horizontal stress of the roof above the roadway decreases rapidly, and the horizontal stress of the roof at 3.5 m exceeds the original rock stress level. The horizontal stress concentration coefficient of the roof at 0.5 m above the coal body is 1.67. With the increase of depth, the stress concentration coefficient decreases rapidly, and there is no significant peak in the stress curve at 3.5 m. As shown in Figure 7(c), the peak shear stress in zone I is significantly higher than that in zone II. When the shear stress in this zone exceeds the shear strength of surrounding rock, a large range of shear failure zone will appear in the upper corners of the roadway. With the increase of the depth, the shear stress in zone I and zone II increases first and then decreases, which indicates the process of the gradual homogenization of the stress distribution.

3.2. Failure Characteristics of Roof. The roadway excavation causes stress disturbance to the natural rock mass, and the stress field of the surrounding rock redistributes. When the stress of surrounding rock exceeds the ultimate bearing capacity of rock mass, the surrounding rock is damaged and the roadway is unstable. Under the action of stress disturbance, the rock usually presents shear failure or tensile shear composite failure. According to Mohr–Coulomb criterion, when the maximum shear stress of the roof rock exceeds its shear strength, the rock mass will undergo shear failure. The maximum shear stress of the roof is

$$\tau_{\max} = \sqrt{\tau_{xz}^2 + \left(\frac{\sigma_x - \sigma_z}{2}\right)^2}. \tag{10}$$

The condition for shear failure of roof is

$$\frac{\left(\left(\sigma_x + \sigma_z/2\right)\tan\varphi + c\right)}{\sqrt{1 + \tan^2\varphi}} \le \tau_{\max}, \tag{11}$$

where φ and c are the internal friction angle and cohesion of the roof rock mass, respectively, and the roof failure criterion can be obtained from equations (10) and (11):

$$F(x, z) = \frac{\left(\left(\sigma_x + \sigma_z/2\right)\tan\varphi + c\right)}{\sqrt{1 + \tan^2\varphi}} - \tau_{\max} \le 0. \tag{12}$$

The failure mode of roof rock mass is drawn by MATLAB, as shown in Figure 8, where $\varphi = 32^\circ$ and $c = 0.5$ MPa. The areas with $F(x, z) \le 0$ in the figure indicate that the roof has been damaged. The roof failure areas above the roadway are symmetrically distributed, and the maximum failure depth is 4.15 m, which is located at the roof above the roadway center line.

According to the failure criterion of roof rock, the stability of roof is related to the stress environment of surrounding rock (σ_x, σ_z, τ_{xz}) and the property of rock mass(c, φ). For a given engineering conditions, it is assumed that the stress environment of the surrounding rock of the roadway is unchanged. Based on the principle of control variables, we take $\varphi = 32^\circ$, $c = 0.5$~3 MPa; $c = 0.5$ MPa, and $\varphi = 25$~39°, and the correlation between the roof failure depth and the rock mass properties is obtained. As shown in Figures 9(a) and 9(b), with the increase of c and φ, the maximum failure depth of roadway roof decreases linearly. Therefore, through reasonable support and reinforcement measures, the mechanical properties of the roof rock mass can be improved and its bearing capacity can be increased, which can greatly improve the stability of the roof and eliminate the hidden danger of roof collapse.

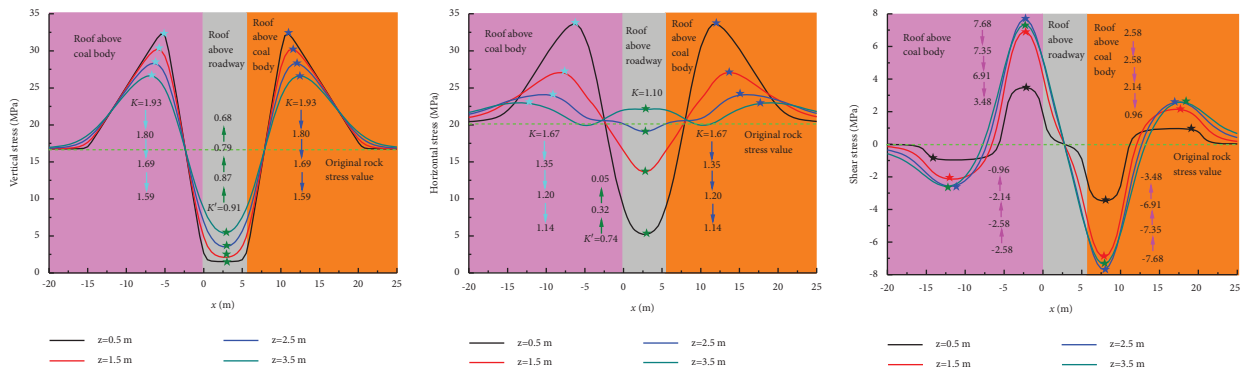

(a) (b) (c)

Figure 7: Roof stress distribution curve: (a) vertical stress; (b) horizontal stress; (c) shear stress.

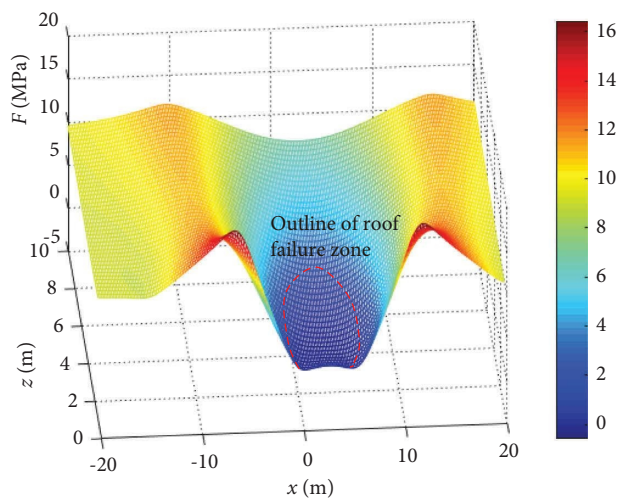

Figure 8: Roof failure characteristics.

4. Stability Analysis of Coal Rib

4.1. Mechanical Model. Under the action of the overlying rock stress, the fracture zone of the coal body in the rib expands, and the split coal body in the shallow potential spalling zone forms a pillar bar structure [22]. We take pillar bar structure as the research object and establish the mechanical model as shown in Figure 10. Since the gravity of pillar bar is far less than the overburden stress, the influence of gravity on its deflection is ignored. According to the static equilibrium conditions, $F_x = qh/2$, where h is the roadway height and q is the uniformly distributed load acting on the pillar bar structure. The bending moment at any section of the pillar bar is

$$M(x) = \frac{1}{2}q(h-x)^2 - \frac{1}{2}qh(h-x) - F_y\omega. \tag{13}$$

According to the deflection differential equation $EI\omega'' = M(x)$, where EI is the stiffness of the pillar bar and ω is its deflection, we can get

$$EI\omega'' = \frac{1}{2}q(h-x)^2 - \frac{1}{2}qh(h-x) - F_y\omega. \tag{14}$$

We set up $\beta^2 = F_y/EI$, and the previous formula can be simplified as

$$\omega'' + \beta^2\omega = \frac{q}{2EI}(h-x)^2 - \frac{qh}{2EI}(h-x). \tag{15}$$

The general solution of the equation can be obtained by solving the previous differential equation, where C_1 and C_2 are undetermined coefficients:

$$\omega = C_1\cos\beta x + C_2\sin\beta x + \frac{q}{2F_y}(h-x)^2 - \frac{qh}{2F_y}(h-x) - \frac{qEI}{F_y^2}. \tag{16}$$

By displacement boundary condition $\omega_{x=0} = 0$, $\omega_{x=h} = 0$, can be obtained as follows: $C_1 = \mathrm{qEI}/F$ and $C_2 = (1-\cos\beta h)\, qEI/(F\sin\beta h)$.

Substituting C_1 and C_2 into formula (4), we can obtain the deflection deformation expression of the pillar bar as follows:

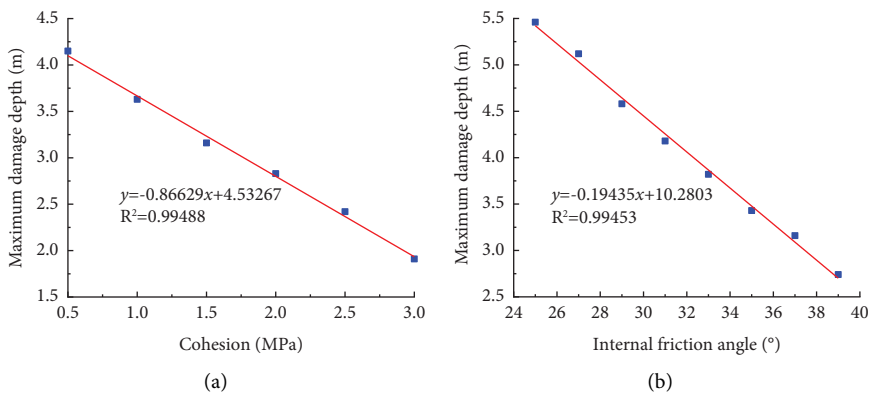

Figure 9: Influencing factors of roof failure depth: (a) cohesion; (b) internal friction angle.

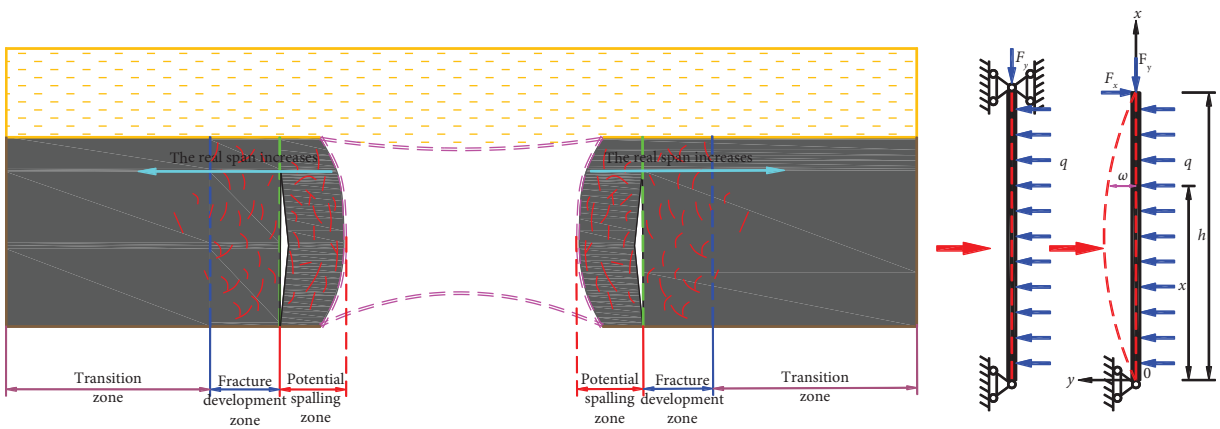

Figure 10: Mechanical model of coal rib.

$$\omega = \frac{qEI}{F_y^{\,2}}\cos\beta x + \frac{qEI}{F_y^{\,2}}\tan\frac{\beta h}{2}\sin\beta x + \frac{q}{2F_y}(h-x)^2 - \frac{qh}{2F_y}(h-x) - \frac{qEI}{F_y^{\,2}}. \tag{17}$$

4.2. Deformation Characteristics of Coal Rib. According to equation (5), based on the control variable method, MATLAB is used to draw the deformation curve of the pillar bar of the coal rib, and the influence of the coal rib stiffness, roof load, roadway height, and lateral load on the stability of the coal rib is obtained, as shown in Figure 11. The deformation in the middle of the coal rib reaches the maximum, and the maximum displacement decreases exponentially with the increase of the stiffness of the coal rib. As shown in Figure 11(a), as the stiffness of the coal rib increases from 10 MN·m^2 to 80 MN·m^2, the maximum displacement decreases by 89.8%; especially, in the range of 10~30 MN·m^2, the response of the coal rib deformation to the change of stiffness is particularly significant. As shown in Figures 11(b) and 11(c), with the increase of roof load and roadway height, the maximum displacement of the coal rib increases exponentially. As the roof load increases from 1 MPa to 6 MPa, the maximum displacement increases from 0.2 m to 1.0 m. As the roadway height increases from 2 m to 7 m, the maximum displacement increases from 0.01 m to 1.6 m. When the roadway height is more than 5 m, the increase of roadway height will promote the maximum displacement significantly. As shown in Figure 11(d), the maximum displacement increases linearly with the increase of lateral load, and the growth rate is 0.41 m/MPa.

To sum up, it is an effective way to control the deformation and failure of the coal rib by actively applying support resistance to it through support units to improve the mechanical properties of the weak structural plane of the coal body and enhance the stiffness of the bearing structure of the coal rib. The roof acts as a medium for the overburden to transmit load to the rib. To improve the stability of the roof, on the one hand, it can limit the transfer of the overburden stress to the coal rib, and at the same time, it can eliminate the hidden danger of roof falling and effectively prevent the secondary increase of the roadway height. After the roadway is excavated, stress concentration occurs at the upper and lower corners. Under the action of concentrated stress, the surrounding rock in these areas is damaged, the pedestal of the pillar bar moves to the deep part of the surrounding rock,

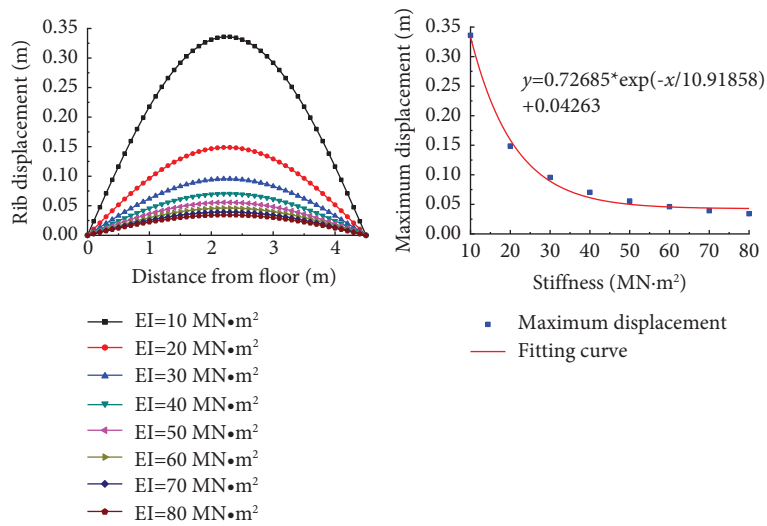

(a)

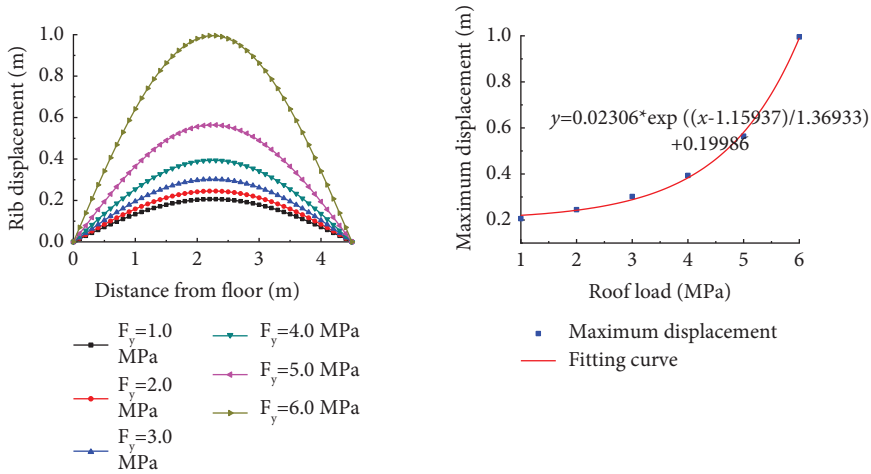

(b)

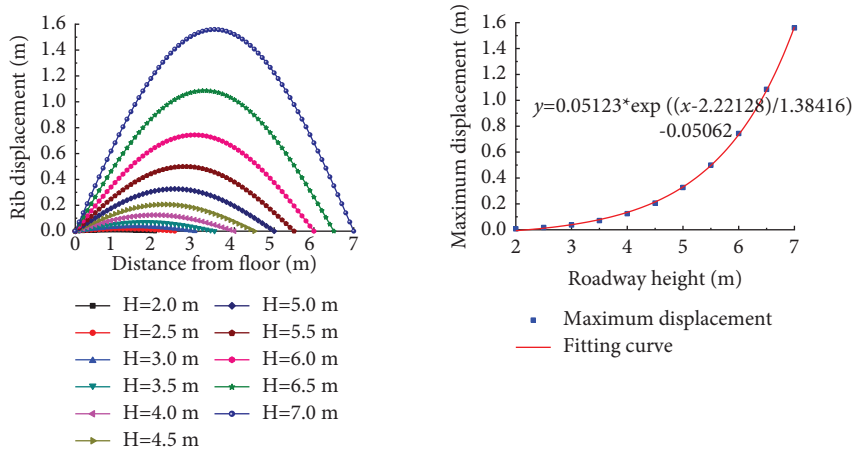

(c)

Figure 11: Continued.

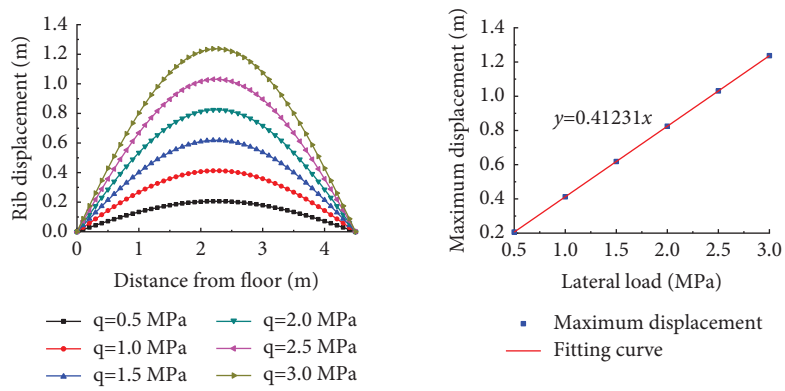

(d)

Figure 11: Deformation characteristics of the coal rib: (a) stiffness effect; (b) roof load effect; (c) roadway height effect; (d) lateral load effect.

and the true height of the roadway increases. Therefore, the control of roadway upper and lower corners has a significant impact on the stability of the coal rib.

5. Surrounding Rock Control Countermeasures and Technology

5.1. Surrounding Rock Control Countermeasures

(1) We build a roof-coal rib-floor coordinated integrated bearing system to improve the overall bearing performance of the surrounding rock support system.

The integrity of layered roof is poor, and the surface of the roof provides a free surface for the release of surrounding rock stress and deformation under engineering disturbance. The roof rock mass shows progressive failure layer by layer from shallow to deep, forming a certain range of potential leakage and falling zone. After the roof is unstable, the true height of the pillar bar increases, and the deformation of the coal rib increases exponentially. The instability of the coal rib will lead to the increase of the true span of the roadway roof and floor and induce roof falling or floor heave. As shown in Figures 13(a) and 13(b), improving the strength of the coal rib can ensure its stable support to the roof rock layer, block the transfer of the load of the overlying rock to the floor, and greatly reduce the overall damage range of the surrounding rock. As shown in Figure 13(c), selecting high-performance bolts and cables to reinforce the roof and floor can restore and maintain the three-dimensional stress state of the rock mass in the fracture zone. As the surrounding rock stress gradually recovers, the radius of Mohr's stress circle decreases. When the stress circle is tangent to the strength envelope, the rock mass reaches the limit equilibrium state. The stress further recovers, and the surrounding rock transits from unstable state to stable state. Each support unit is coupled to each other and carries loads cooperatively, so as to build a roof-coal rib-floor coordinated integrated bearing system and improve the integrity of the bearing system.

(2) Grouting fills the internal cracks of surrounding rock and improves the overall bearing capacity of weak and broken coal and rock mass.

Grouting can strengthen the loose and broken coal and rock mass, fill the cracks of surrounding rock, and improve its mechanical properties and bearing capacity. At the same time, the grouting reinforcement zone provides a reliable force foundation for the bolts and cables to ensure the full play of their anchoring efficiency.

(3) Full section shotcrete is used to prevent the deterioration of surrounding rock strength caused by water rich environment.

The full section shotcrete seals the surrounding rock, fills the cracks on the surface of the surrounding rock, blocks the water seepage channel from the roof to the inside of the surrounding rock, and prevents the surrounding rock from weathering and swelling when encountering water. At the same time, the shotcrete layer bonds the surrounding rock and the supporting units into a unified supporting structure, which can give full play to the self-bearing capacity of the surrounding rock.

5.2. Surrounding Rock Control Technology. In view of the deformation and failure characteristics of the roof and floor, based on the above surrounding rock control measures, taking the south return air main roadway of Zhaozhuang Mine as the engineering background, the support parameters are optimized through engineering analogy, theoretical analysis, and numerical calculation, and the rib strengthening and roof controlling coordinated integrated support technology based on high-strength prestressed cables, and deep and shallow hole grouting is proposed, as shown in Figure 13. Specific support parameters are as follows:

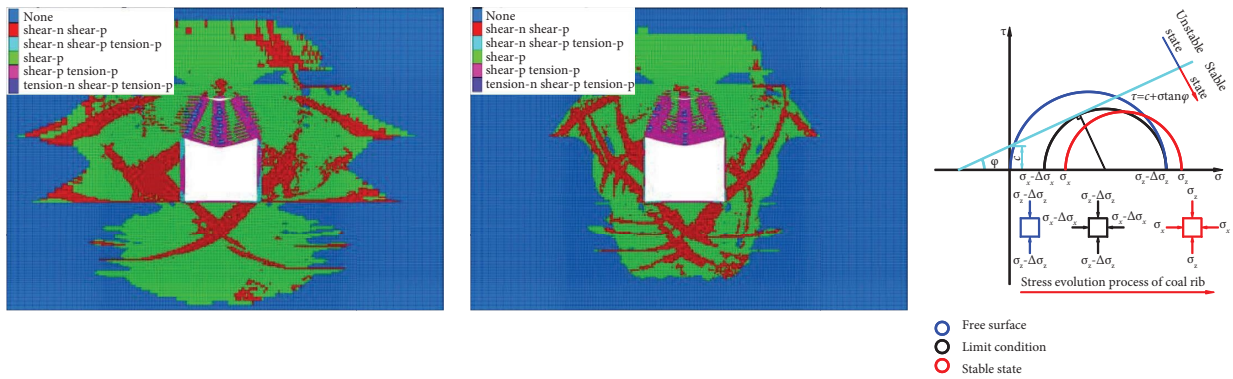

(a) (b) (c)

Figure 12: Influence of the rib bearing capacity: (a) weak rib; (b) strong rib; (c) stress evolution process.

(1) *Roof and Rib Cooperative Control Technology.* Layered soft roof has high risk of roof falling and is easy to form ultrahigh roadway. The treatment of this kind of roadway must consider the overall stability of the roof-coal rib-floor bearing system. Selecting high-performance bolts and cables components, exerting sufficient pretightening force and support in time are the keys to achieving roadway stability.

As shown in Figures 13(a) and 13(b), SKP22-1/1720-7400 high-strength low relaxation steel strand is used for roof cables, and the spacing is 1000 mm × 1200 mm, with 5 cables arranged in each row. The anchorage length of the cable is 1970 mm, and the pretightening force is not less than 250 kN. Each row of anchor cables shall be connected by steel beam. As shown in Figure 13(c), A MSGLW-500/22-3200 high-strength left-handed nonlongitudinal rebar threaded steel bolt is arranged at the upper corner and lower corner of the rib, respectively. The bolt row spacing is 1200 mm, with a deflection angle of 10° and an anchorage length of 1675 mm, and the tightening torque is not less than 400 N·m. SKP22-1/1720-5400 high-strength low relaxation steel strand is used for rib cables, and the spacing is 950 mm × 1200 mm, with 3 cables arranged in each row. The anchorage length of the cable is 1970 mm, and the pretightening force is not less than 250 kN. The stiffness of the surface floor has an important influence on the deformation of the layered floor. The hardening of the floor is realized by pouring concrete, which can improve the deformation resistance of the floor, and seal the floor at the same time, so as to avoid the deterioration of the rock strength of the floor caused by the water pouring from the roof. The design thickness of the roadway concrete floor is 200 mm, and the concrete strength grade is C20.

(2) *Deep and Shallow-Hole Grouting Technology.* The weak and broken rock mass has poor integrity and low bearing capacity, and the bolts and cables cannot form an effective force foundation, which limits the full play of the support efficiency of the support units. The deep and shallow-hole grouting technology is used to restore the mechanical properties of the shallow one surrounding rock, improve the bearing capacity of the deep rock mass, and cooperate with the corresponding support means to reduce the risk of roof falling and rib spalling.

The specifications of shallow grouting holes are Φ30 × 1500 mm, and the grouting pressure is 0.8–1.0 MPa. We keep the grouting pressure for about 15 minutes, close the valve, and block the grouting hole. The specifications of deep grouting holes are Φ30 × 5000 mm. The initial grouting pressure is 0.8–1.0 MPa, which gradually increases the grouting pressure. When the grouting pressure reaches 3-4 MPa, we maintain the pressure grouting for 20 minutes, close the valve, and end the grouting.

(3) *Full-Section Shotcrete Sealing Surrounding Rock Technology.* Underground roadways exist in humid and hot engineering environment, and surrounding rocks are easy to be weathered and broken [23]. Shotcreting can fill the cracks on the roadway surface, seal the surrounding rock, and prevent the surrounding rock from weathering and swelling when encountering water. At the same time, the shotcrete layer bonds the surrounding rock and the supporting units into a unified supporting structure, which can give full play to the bearing capacity of the surrounding rock itself. After the support is completed, C20 concrete layer with thickness of 150 mm should be sprayed on the roof and rib.

6. Support Reliability Evaluation

6.1. Evaluation by Numerical Calculation. A single bolt or cable forms a certain range of support stress field in its anchoring area. By reasonably controlling the spacing of support units, the support stress fields of each bolt and cable can be superimposed on each other, so as to form a certain range of compression zone in the surrounding rock (Figure 14(a)). The property and integrity of rock mass in this area are improved,

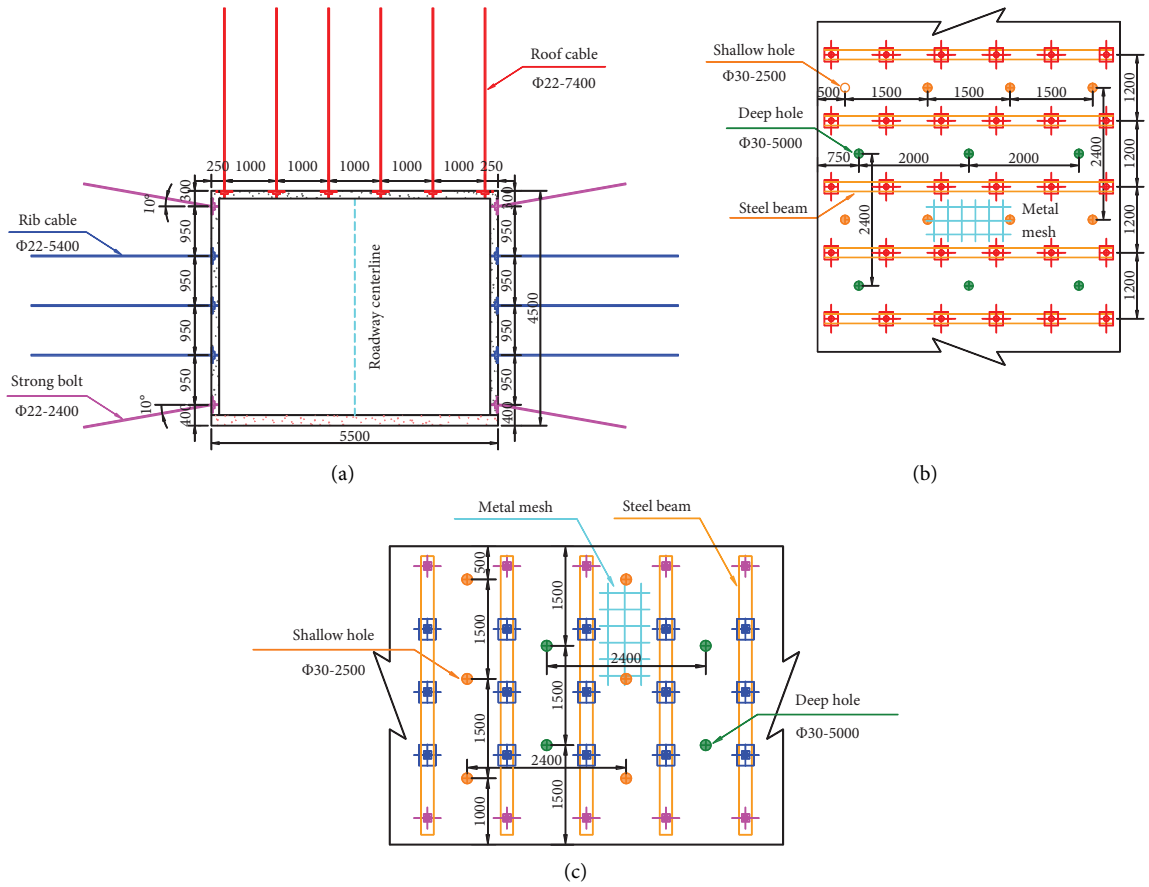

Figure 13: Roadway support parameters: (a) full section; (b) roof; (c) rib.

and the bearing capacity of surrounding rock is enhanced. As shown in Figures 14(b) and 14(c), grouting reinforcement and support improve the mechanical properties of weak structural planes and enhance the antisliding ability between layers. The layered roof changes from composite beam structure to composite beam structure, and the potential roof falling arch disappears. The supporting units that reach the stable rock mass are coupled with the surrounding rock to form a roof-coal rib-floor coordinated bearing system, which greatly improves the overall stability of the roadway, diminishes the damage range of the surrounding rock, reduces the potential risk of roof falling, and prevents the formation of ultrahigh roadway.

6.2. Engineering Application Effect. After the roadway is excavated, support is carried out in time, and rock pressure measuring stations are arranged to evaluate the surrounding rock control effect (Figure 15(a)). Dynamometer is used to monitor the stress of the bolts and cables in the working process, multipoint displacement meter is used to monitor the internal deformation of surrounding rock, and laser rangefinder and steel tape are used to monitor the roadway surface displacement. The stress variation trend of the bolts and cables is shown in Figure 15(b). During the monitoring period, the stress of the bolts and the cables increased synchronously, and there was no sharp increase in the stress, nor was there any failure of the component and the stress returned to zero, indicating that the bolts and the cables and the surrounding rock reached a synergistic coupling bearing state. The stress of the bolts and cables arranged at the upper corner increases sharply, which indicates that the support units play a good role in controlling the weak zone and avoid the overall instability of the roadway caused by the damage of local weak zones.

The roadway surface displacement curve is shown in Figure 15(c). After the excavation of the roadway, the surrounding rock enters a period of severe deformation, and the deformation of the surrounding rock increases rapidly. As the supporting units and surrounding rock form a cooperative bearing structure, the surrounding rock enters a stable deformation period, and the deformation speed tends to be stable. After 40 days, the surrounding rock enters a stable period, and the deformation of the surrounding rock basically does not increase. The accumulated deformation of roof, floor and rib is 68 mm, 46 mm, and 148 mm, respectively. The convergence deformation of the roadway is small and the overall stability is good.

The deformation curve of rock mass in different layers of roof is shown in Figure 15(d). The supporting efficiency of roof cables improves the deformation resistance of the shallow roof (1 m base point), and the accumulated deformation in this area is 43 mm. With the increase of roof

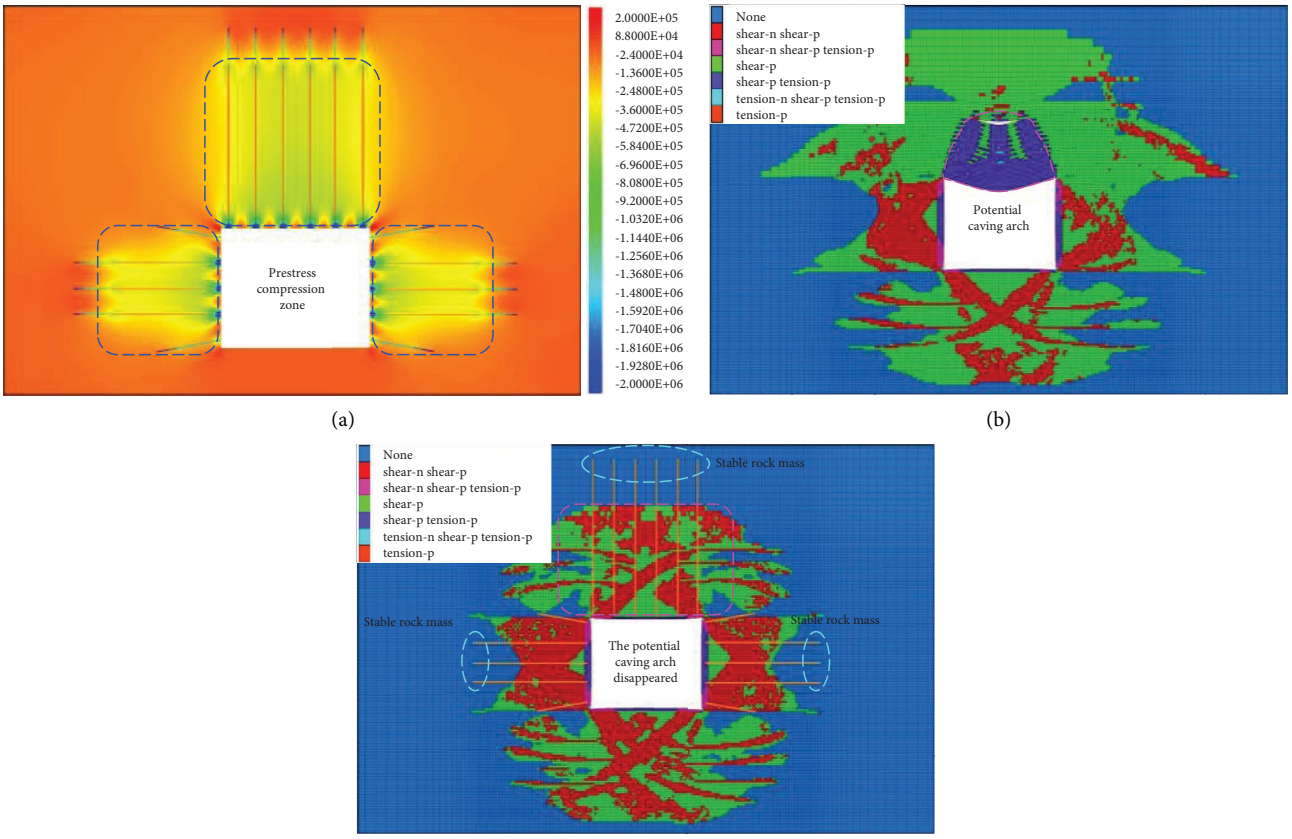

Figure 14: Numerical simulation results: (a) support stress field; (b) unsupported roadway; (c) supported roadway.

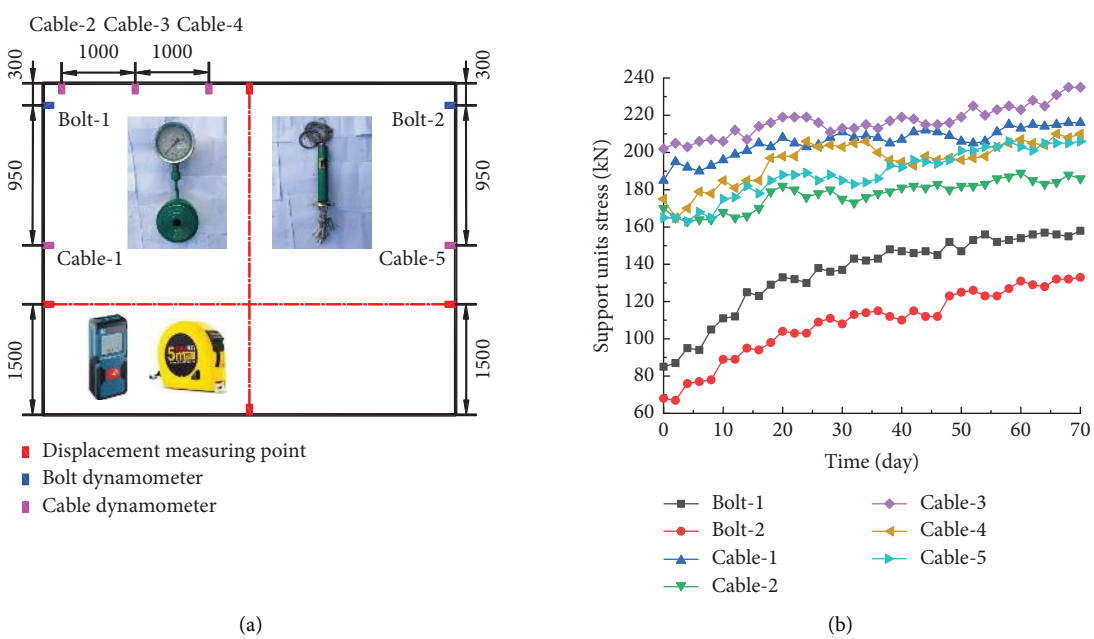

Figure 15: Continued.

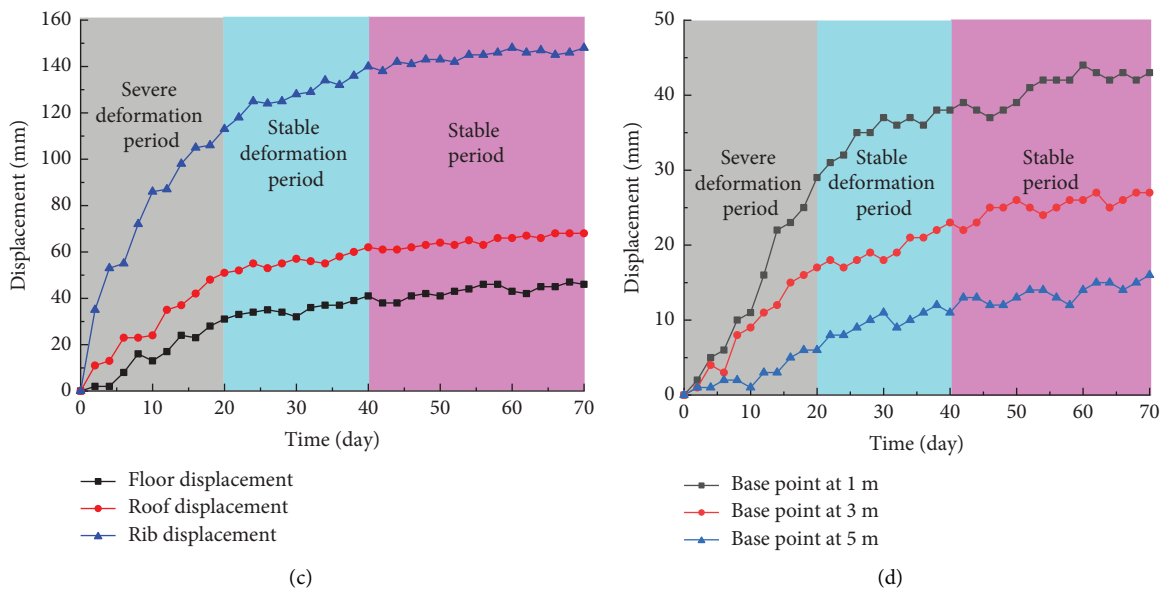

Figure 15: Monitoring results: (a) layout of monitoring station; (b) stress curve of bolts and cables; (c) roadway surface deformation; (d) internal deformation of surrounding rock.

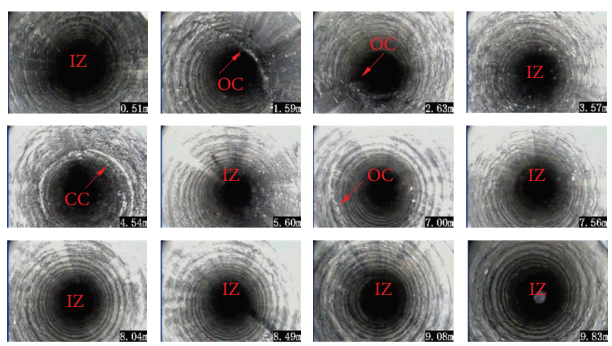

Figure 16: Borehole imaging results of roof (OC means open crack; CC means circumferential crack; IZ means intact zone).

depth, the stability of roof improves. The cumulative deformation of the roof at 3 m and 5 m is 27 mm and 16 mm, respectively. The monitoring results show that the deep and shallow-hole grouting and prestressed cables support greatly improve the bearing capacity of the layered roof, form a stable bearing structure from shallow to deep, and effectively reduce the hidden danger of roof falling.

After the roadway was excavated for 5 months, the internal structure of the roof was detected by borehole imaging technology. As shown in Figure 16, the support scheme effectively controls the evolution of roof cracks. Only a few open fractures can be seen locally, and the fractures do not penetrate each other to form a fracture zone. The overall stability of the roof is good. The roof separation is effectively controlled, which suppresses the formation of roof caving zone, thus eliminating the formation of ultrahigh roadway from the source.

7. Conclusions

In this paper, in order to prevent the occurrence of ultrahigh roadway caused by roof falling in Zhaozhuang Mine, the cooperative integrated support technology based on high-strength prestressed cables and deep-shallow hole grouting is proposed. Through theoretical analysis, numerical simulation and field test, the reliability of support technology is proved. The following main conclusions are drawn:

(1) After the roadway is excavated, the layered roof forms potential leakage and falling zone, metastable zone, and stable zone from shallow to deep. The roof shows obvious progressive failure layer by layer, forming a potential caving arch structure. The weak coal rib forms potential spalling zone, crack developed zone, and transition zone. The damage of the coal rib increases the true span of the roadway and further reduces the stability of the roof. The gradual development of rock layers separation within the potential caving arch induces the structural instability of rock mass within the arch, leading to roof caving and finally forms an ultrahigh roadway with a height of about 7~8 m.

(2) The coal bearing rock series formed a typical layered structure during the deposition process. The mechanical behavior of layered rock mass is affected by

the weak structural plane and has significant anisotropy. The layered roof is regarded as a transversely isotropic body. Based on the elastic theory, the mechanical model of layered roof is established. According to the superposition principle, the real stress state of any point of the layered roof is deduced, which accurately reflects the stress distribution characteristics of the layered floor.

(3) Based on Mohr–Coulomb criterion, the failure criterion of layered roof is established. The symmetrical failure mode of roof rock mass is plotted by MATLAB, and the theoretical solution of the failure depth of layered roof is obtained. Based on the principle of control variables, the maximum failure depth of roof decreases linearly with the increase of rock mass properties.

(4) The pillar bar mechanical model of the potential spalling zone is established, and the expression of the deflection deformation of the pillar bar is derived. Based on the principle of control variable, the maximum deformation of coal rib decreases exponentially with the increase of its stiffness, increases exponentially with the increase of roof load and roadway height, and increases linearly with the increase of lateral load.

(5) In view of the deformation and failure characteristics of the roof and coal rib, this paper puts forward the cooperative integrated support technology based on high-strength prestressed cables and deep-shallow hole grouting. The results of numerical calculation and field observation show that the designed support scheme can effectively reduce the hidden danger of roof falling and eliminate the formation of ultrahigh roadway from the source.

Data Availability

The data used to support the findings of the study are available from the corresponding author upon request.

Disclosure

The data results analyzed in this paper are true and reliable.

Conflicts of Interest

The authors declare that they have no conflicts of interest.

Acknowledgments

This paper was supported by the Anhui University of Science and Technology high-level talent research startup fund (Grant no. 2021yjrc39), the National Natural Science Foundation of China (Grant no. 52204122), the Open Fund of the State Key Laboratory for Mining Response and Disaster Prevention and Control in Deep Coal Mines (Grant no. SKLMRDPC21KF14), and the Institute of Energy, Hefei Comprehensive National Science Center (Grant no. 21KZS217).

References

[1] H. P. Kang, J. Lou, F. Gao, J. Yang, and J. Li, "A physical and numerical investigation of sudden massive roof collapse during longwall coal retreat 1mining," *International Journal of Coal Geology*, vol. 188, pp. 25–36, 2018.

[2] F. Gao and D. Stead, "Discrete element modelling of cutter roof failure in coal mine roadways," *International Journal of Coal Geology*, vol. 116-117, pp. 158–171, 2013.

[3] F. Gao, D. Stead, and H. P. Kang, "Simulation of roof shear failure in coal mine roadways using an innovative UDEC trigon approach," *Computers and Geotechnics*, vol. 61, pp. 33–41, 2014.

[4] R. Gu and U. Ozbay, "Distinct element analysis of unstable shear failure of rock discontinuities in underground mining conditions," *International Journal of Rock Mechanics and Mining Sciences*, vol. 68, pp. 44–54, 2014.

[5] Y. An, N. Zhang, Y. M. Zhao, and Z. Xie, "Field and numerical investigation on roof failure and fracture control of thick coal seam roadway," *Engineering Failure Analysis*, vol. 128, Article ID 105594, 2021.

[6] Q. S. Bai, S. H. Tu, C. Zhang, and D. Zhu, "Discrete element modeling of progressive failure in a wide coal roadway from water-rich roofs," *International Journal of Coal Geology*, vol. 167, pp. 215–229, 2016.

[7] Y. Yu, X. Y. Wang, J. Bai, L. Y. Zhang, and H. C. Xia, "Deformation mechanism and stability control of roadway surrounding rock with compound roof: research and applications," *Energies*, vol. 13, no. 6, p. 1350, 2020.

[8] L. S. Jiang, H. S. Mitri, N. J. Ma, and X. D. Zhao, "Effect of foundation rigidity on stratified roadway roof stability in underground coal mines," *Arabian Journal of Geosciences*, vol. 9, no. 1, pp. 32–12, 2016.

[9] X. Liu, X. Hua, P. Yang, and Z. Huang, "A study of the mechanical structure of the direct roof during the whole process of non-pillar gob-side entry retaining by roof cutting," *Energy Exploration & Exploitation*, vol. 38, no. 5, pp. 1706–1724, 2020.

[10] Y. Yu, J. Lu, D. Chen, Y. Pan, X. Q. Zhao, and L. Y. Zhang, "Study on the stability principle of mechanical structure of roadway with composite roof," *Minerals*, vol. 11, no. 9, p. 1003, 2021.

[11] F. Gao, D. Stead, and H. P. Kang, "Numerical simulation of squeezing failure in a coal mine roadway due to mining-induced stresses," *Rock Mechanics and Rock Engineering*, vol. 48, no. 4, pp. 1635–1645, 2015.

[12] H. W. Wang, S. Xue, Y. D. Jiang, D. X. Deng, S. Shi, and D. Zhang, "Field investigation of a roof fall accident and large roadway deformation under geologically complex conditions in an underground coal mine," *Rock Mechanics and Rock Engineering*, vol. 51, no. 6, pp. 1863–1883, 2018.

[13] X. Sun, L. Wang, Y. Lu, B. Jiang, Z. Li, and J. Zhang, "A yielding bolt-grouting support design for a soft-rock roadway under high stress: a case study of the Yuandian No. 2 coal mine in China," *Journal of the South African Institute of Mining and Metallurgy*, vol. 118, no. 1, pp. 71–82, 2018.

[14] W. Wu, J. Bai, X. Y. Wang, S. Yan, and S. X. Wu, "Numerical study of failure mechanisms and control techniques for a gob-side yield pillar in the sijiazhuang coal mine, China," *Rock Mechanics and Rock Engineering*, vol. 52, no. 4, pp. 1231–1245, 2019.

[15] L. De-Feng, B. Guo, L. Chang-wu, Y. Kang, L. I. Jia-feng, and Y. Jiang, "Analysis of limit equilibrium zone for roadway side wall considering engineering disturbance and geological

condition," *Journal of China Coal Society*, vol. 42, no. 3, pp. 597–603, 2017.

[16] W. De-chao, W. Hong-tao, L. I. Shu-cai, Q. Wang, and S. Yang, "Stress and deformation analysis of the side wall in a roadway driven along goaf incorporating the strength softening characteristics of coal mass," *Journal of China University of Mining & Technology*, vol. 48, no. 2, pp. 295–304, 2019.

[17] S. Ren-liang, X. S. Kong, Y. Fa-yuan, and C. Meng, "Research on sidewall and corner strengthened support for coal roadway by modeling experiments," *Chinese Journal of Rock Mechanics and Engineering*, vol. 34, no. 11, pp. 2336–2345, 2015.

[18] S. Ren-liang, X. S. Kong, W. Zhen-ting, L. I. Min-zu, S. J. Yang, and L. Tian, "Theory and application of strong support for coal roadway sidewall," *Chinese Journal of Rock Mechanics and Engineering*, vol. 32, no. 7, pp. 1304–1314, 2013.

[19] H. Wu, Q. Jia, W. Wang, N. Zhang, and Y. Zhao, "Experimental test on nonuniform deformation in the tilted strata of a deep coal mine," *Sustainability*, vol. 13, no. 23, Article ID 13280, 2021.

[20] H. Lu and D. X. Yao, "Stress distribution and failure depths of layered rock mass of mining floor," *Chinese Journal of Rock Mechanics and Engineering*, vol. 33, no. 10, pp. 2030–2039, 2014.

[21] Y. Zhu, Y. Li, and W. Li, "Stability analysis of layered floor affected by multiple mining activities in the whole service life," *Arabian Journal of Geosciences*, vol. 16, no. 1, p. 80, 2023.

[22] Q. X. Huang and J. H. Liu, "Vertical slice model for coal wall spalling of large mining height longwall face in shallow seam," *Journal of Mining & Safety Engineering*, vol. 32, no. 02, pp. 187–191, 2015.

[23] W. Yu, K. Li, Z. Liu, B. An, P. Wang, and H. Wu, "Mechanical characteristics and deformation control of surrounding rock in weakly cemented siltstone," *Environmental Earth Sciences*, vol. 80, no. 9, Article ID 337, 2021.